ASCE

Mechanisms of Alkali-Silica Reaction Mitigation in AMBT Conditions: Comparative Study of Traditional Supplementary Cementitious Materials

Marie Joshua Tapas, Ph.D.[1]; Paul Thomas, Ph.D.[2]; Kirk Vessalas, Ph.D.[3]; and Vute Sirivivatnanon, Ph.D.[4]

Abstract: This study investigates the mechanisms of alkali-silica reaction (ASR) mitigation by supplementary cementitious materials (SCMs) under accelerated mortar bar test (AMBT) conditions. The study compares the effect of traditional SCMs (fly ash, slag, metakaolin, and silica fume) on ASR expansion, calcium silicate hydrate (C-S-H) composition, and portlandite consumption as well as on the availability of silicon and aluminum in solution. Results show that at typical SCM replacement levels for effective ASR mitigation (15% metakaolin, 25% fly ash, and 65% slag), the Si/Ca and Al/Si ratios of C-S-H are increased to comparable values, suggesting that at these dosages the SCMs contribute almost equivalent amounts of silicon and aluminum in solution. Studies of blended cement + SCM pastes show that the order of pozzolanicity is as follows: silica fume > metakaolin > fly ash > slag, which is consistent with the order of efficacy of SCMs in mitigating ASR expansion and the measured concentrations of silicon in solution. Solubility studies of the SCMs showed formation of sodium aluminum silicate hydrate (N-A-S-H) in fly ash and metakaolin and formation of calcium aluminum silicate hydrate (C-A-S-H) in slag after 28 days of exposure to AMBT conditions. This highlights the role of alkali activation of SCMs in ASR mitigation under AMBT conditions.
DOI: 10.1061/(ASCE)MT.1943-5533.0004097.

Author keywords: Alkali-silica reaction (ASR); Supplementary cementitious materials (SCM); Fly ash; Slag; Dissolution; Accelerated mortar bar test (AMBT); Silica fume; Metakaolin.

Introduction

Alkali-silica reaction (ASR) is a phenomenon characterized by the dissolution of reactive siliceous components of aggregates followed by formation of a hygroscopic gel that expands as it absorbs moisture, resulting in cracking when the tensile stresses generated exceed the tensile strength of the concrete (Rajabipour et al. 2015). Three factors are essential to ASR: reactive silica (SiO_2) in aggregates (i.e., SiO_2 minerals that are strained, contain defects, have poor crystallinity, or are amorphous in nature), a highly alkaline pore solution, and sufficient moisture to allow the dissolution precipitation reactions to occur (Rajabipour et al. 2015).

The use of a nonreactive aggregate is no doubt the safest mitigation approach to prevent the occurrence of ASR. However, due to geographical constraints or local unavailability, using nonreactive aggregates is not always an option. Incorporating supplementary cementitious materials (SCMs) such as fly ash (FA), ground-granulated blast-furnace slag (SL), metakaolin (MK), and silica fume (SF) in the concrete mix is therefore widely regarded as the most economical means of preventing ASR (Thomas 2011). The presence of SCMs allows the use of reactive aggregates that may not be otherwise suitable for concrete structures.

The commonly used SCMs fly ash, slag, and silica fume are industrial by-products. Fly ash is generated from burning coal at electrical power stations, slag is a by-product of steel production from iron ore, and silica fume is a by-product from the production of ferrosilicon metals (Thomas 2013). Hence, supply is highly limited and dependent on the frequency of the production. The global drive to close coal-fired power stations in an effort to reduce CO_2 emissions particularly threatens the supply of fly ash (Johnson and Chau 2019; Nalbandian-Sugden 2015). The slag supply also faces shortage, with current supply estimated to be only about 8% of total cement production (Scrivener et al. 2016). A better understanding of the mechanisms by which SCMs function is therefore critical in the identification and assessment of future SCMs. The use of metakaolin and silica fume in Australia is very limited due to their much higher cost.

The widely accepted mechanism by which SCMs mitigate ASR is by reducing the alkalinity of the pore solution (Duchesne and Berube 1994b). The reactive silica present in SCMs reacts with the hydroxyl ions in the pore solution and portlandite (CH) to produce calcium silicate hydrate (C-S-H) phases that have a decreased Ca/Si ratio, which causes more alkali ions to be entrapped in the hydrates (Duchesne and Berube 1994b; Durand et al. 1990; Hong and Glasser 1999; Kim et al. 2015; Thomas 2013). Studies by Hong and Glasser (2002) and Lothenbach et al. (2011) suggested that the aluminium in SCMs can also dissolve into the pore solution

[1]Research Associate, School of Civil and Environmental Engineering, Univ. of Technology Sydney, 81 Broadway, Ultimo, NSW 2007, Australia (corresponding author). ORCID: https://orcid.org/0000-0003-0575-1113. Email: mariejoshua.tapas@uts.edu.au

[2]Senior Lecturer, School of Mathematical and Physical Sciences, Univ. of Technology Sydney, 81 Broadway, Ultimo, NSW 2007, Australia. Email: Paul.thomas@uts.edu.au

[3]Senior Lecturer, School of Civil and Environmental Engineering, Univ. of Technology Sydney, 81 Broadway, Ultimo, NSW 2007, Australia. ORCID: https://orcid.org/0000-0003-3948-5212. Email: kirk.vessalas@uts.edu.au

[4]Professor, School of Civil and Environmental Engineering, Univ. of Technology Sydney, 81 Broadway, Ultimo, NSW 2007, Australia. Email: Vute.sirivivatnanon@uts.edu.au

Note. This manuscript was submitted on January 28, 2021; approved on June 25, 2021; published online on December 17, 2021. Discussion period open until May 17, 2022; separate discussions must be submitted for individual papers. This paper is part of the ***Journal of Materials in Civil Engineering***, © ASCE, ISSN 0899-1561.

and be further incorporated into the pozzolanic reactions to form C-A-S-H (also known as Al-modified C-S-H) gel that has enhanced alkali binding capacity (Hong and Glasser 2002; Lothenbach et al. 2011). The incorporated aluminum in the silanol layer leads to a free negative valence, resulting in the compensation of this charge by the positive alkali ions Na^+ and K^+.

The required dosage for effective mitigation depends on the type of SCM (Boddy et al. 2003; Durand et al. 1990; Thomas 2011). In Australia, SA HB 79:2015 provides recommended replacement levels of SCMs to mitigate ASR. Slag requires the highest amount of replacement at 65%, followed by fly ash (Class F) at 25%, metakaolin at ≤15%, and silica fume at 10% (Standards Australia 2015).

Two test methods are widely used to assess aggregate reactivity and the efficacy of SCMs in ASR mitigation: the accelerated mortar bar test (AMBT) and the concrete prism test (CPT). The more rapid test method AMBT involves monitoring expansion of mortar specimens immersed in 1 M NaOH at 80°C, while the longer test method CPT involves measuring expansion of concrete specimens boosted with alkali to reach 1.25% Na_2O_{eq} and stored in a 38°C high-humidity environment. The most popular versions of these test methods include American standards ASTM C1567 (ASTM 2013) (AMBT) and ASTM C1293 (ASTM 2020) (CPT). Australia also has its own version of these test methods, AS 1141.60.1 (Standards Australia 2014b) (AMBT) and AS 1141.60.2 (Standards Australia 2014c) (CPT), which are very similar to the American standards but slightly differ in the test limits. Despite the limitations of AMBT owing to its high alkali concentration and high-temperature conditions, including its inability to detect the influence of cement alkalis on ASR expansion (low-alkali cements in particular, hence limiting its application for determining alkali threshold) (Islam et al. 2016; Tapas et al. 2021b; Thomas et al. 2006), it is still the most popular test method in Australia due to the fast turnaround time of just 21 days and its relatively good performance in screening nonreactive aggregates (Sirivivatnanon et al. 2016; Standards Australia 2015). Numerous studies have also correlated AMBT results to field data and have reported that the outcome agrees well and that the combination of aggregates and SCMs that pass the AMBT test limit have very low potential for ASR (Hooton et al. 2013; Thomas et al. 2012, 2011, 2007).

Owing to the popularity of AMBT despite its limitations, its effect on ASR mitigation and SCM behavior is of high interest. It has been reported that in AMBT, fly ash mitigates ASR by alkali binding, mass transport reduction, increasing the tensile strength, and reducing the aggregate dissolution rate (Shafaatian et al. 2013). Mortars with fly ash after 3 days of submersion in 1 M NaOH at 80°C (ASTM C1567) exhibit higher tensile and compressive strength than control mortars. The high early-age strength, which is attributed to increased rate of pozzolanic reactions due to higher temperature and alkalinity, delays the formation of cracks, which can promote immediate access of the NaOH solution to the interior of the specimen. Further, in their experiment where glass slides were immersed in alkali with and without fly ash in solution, it was observed that the rate of mass loss from glass slides is higher in the system without fly ash. The authors attribute this to a drastic increase in the silicate surface area to solution volume ratio as a result of the silicate area provided by the fly ash resulting in a much lower concentration of OH^- ions per unit silicate surface area (Shafaatian et al. 2013). A study of the pore solutions of mortars with silica fume and fly ash further confirmed that despite access to an unlimited supply of alkalis, mortars with SCMs exhibit much lower alkali concentration that the 1 M NaOH storage solution during the 14-day test period (Berube et al. 1995). Although there have been a few investigations on the mechanisms behind SCM mitigation during AMBT, there is still no study that has clearly demonstrated the effect of various SCMs on the C-S-H composition of mortar bars post-AMBT (at recommended SCM replacements for effective ASR mitigation) as well as the alkali activation of SCMs when exposed to alkaline media and elevated temperature similar to AMBT.

This study aims to investigate the mechanisms of ASR mitigation in AMBT using traditional SCMs (fly ash, slag, metakaolin, and silica fume) by correlating ASR expansion with the composition of the C-S-H phases of mortar specimens post-AMBT and portlandite consumption of cement + SCM blends, as well as the release of silicon and aluminum from SCMs after exposure to AMBT conditions. The products formed by the SCMs under AMBT exposure conditions were also characterized to provide better insight into the beneficial role of the alkali activation of SCMs on ASR mitigation under AMBT conditions as well as the competitive nature between sodium and calcium.

Materials and Methods

Raw Materials

Cement, aggregate, and SCMs used in this study were sourced in Australia. Cement Concrete and Aggregates Australia (CCAA, Mascot, New South Wales, Australia), which is the primary body for the heavy construction materials industry in Australia, supplied the reactive aggregate graywacke, while cement and SCMs were supplied by Cement Australia (Darra, Queensland, Australia). The oxide compositions of cement, SCMs, and aggregate utilized measured using X-ray fluorescence (XRF) (PANalytical PW2400, Malvern, United Kingdom) are listed in Table 1. Table 2 provides the mineralogical composition of reactive aggregate graywacke as determined by petrographic analysis carried out in accordance with Australian standard AS 2758.1 (Standards Australia 2014a) and ASTM C295 (ASTM 1990) by Geochempet Services, Brisbane Australia.

ASR Expansion Test

The effect of substituting a portion of the cement with SCMs on ASR mitigation was evaluated using AMBT. Mortar bars composed of 1 part cement to 2.25 parts graded aggregate by mass (440 g cement per 990 g of aggregate) and water to cementitious materials ratio equal to 0.47 were prepared in accordance with AS 1141.60.1. The SCMs were used at industry replacement dosages: fly ash (15% and 25%), slag (35% and 65%), metakaolin (10% and 15%), and silica fume (5% and 10%) (Standards Australia 2015).

Table 1. XRF analysis of the cement, SCMs, and aggregate (% by weight)

Oxide	General portland cement	Fly ash	Slag	Metakaolin	Silica fume	Graywacke
SiO_2	19.67	59.21	34.12	62.5	91.46	66.85
TiO_2	0.22	1.11	0.87	1.02	0.01	0.65
Al_2O_3	4.78	28.11	14.37	32.39	0.1	14.24
Fe_2O_3	3.10	3.68	0.3	0.82	0.01	3.8
Mn_3O_4	0.12	0.11	0.36	0.01	0.02	0.09
MgO	0.91	0.53	5.31	0.67	0.7	1.58
CaO	64.18	2.48	41.59	0.07	0.24	1.94
Na_2O	0.33	0.63	0.35	0.22	0.28	4.25
K_2O	0.41	1.18	0.26	0.28	0.52	3.11
P_2O_5	0.06	0.41	0.01	0.03	0.14	0.14
SO_3	2.37	0.16	2.83	0.08	0.07	0.19
Loss on ignition	4.09	1.05	0.35	1.75	5.55	2.29

Table 2. Graywacke mineralogical composition

Mineral	Percentage
Microcrystalline feldspars	37
Microcrystalline quartz	17
Quartz	13
Epidote	8
Moderately strained quartz	7
Feldspar	7
Lithic clasts	5
Calcite	3
Chlorite	2
Sericite	1

Table 3. AMBT expansion criteria

Mean mortar bar expansion (%)		
Duration of specimens in 1M NaOH 80°C		Reactivity classification
10 days	21 days	
—	$E < 0.10$	Nonreactive
$E < 10$	$0.10 \le E < 0.30$	Slowly reactive
$E \ge 0.10$	—	Reactive
—	$0.30 \le E$	Reactive

Source: Data from AS 1141.60.1.

Additional mortars with 10% SCM replacement level of fly ash and slag were also prepared for purposes of comparison with lower replacement dosages of metakaolin and silica fume.

The mortar specimens were prepared on $25 \times 25 \times 285$ mm molds with a gauge length of 250 mm, then cured in a high-humidity environment at room temperature (23°C ± 2°C) for 24 h. After, the specimens were demolded and placed in a container filled with water. The container was subsequently placed in an oven set at 80°C for another 24 h to allow the specimens to slowly equilibrate to 80°C. A horizontal comparator was used to obtain zero-hour length measurements before immersing the specimens in 1 M NaOH solution at 80°C for 28 days. Succeeding expansion measurements were obtained at 1, 3, 7, 10, 14, 21, and 28 days. Three readings were taken per mortar specimen at each age.

Total expansions incurred by the aggregate after 10 and 21 days of NaOH immersion were used to classify its ASR potential when used in the field in accordance with AS 1141.60.1. Because Australia does not have an existing standard for assessing the efficacy of SCMs in ASR mitigation, the same criteria were employed for mixes with SCMs because it is very similar to the widely accepted ASTM C1567 (ASTM 2013). The classification criteria are listed in Table 3.

Analysis of Mortar Bars Post-AMBT

The mortar specimens were sectioned for microstructural analysis. The mortars were cut with a diamond saw and then placed in a container with isopropanol for 7 days to remove free water (fully immersed to facilitate solvent exchange). Then the cut mortars were molded in epoxy resin and polished using a Struers automated polishing machine (Cleveland). MD Largo disk and various sizes of diamond sprays (9, 3, and 1 μm) were used to ensure optimal polishing quality. The polished sections were allowed to dry in a vacuum desiccator for 2 days prior being subjected to imaging and elemental analysis.

FEI Quanta 200 (Hillsboro, Oregon) with Bruker XFlash 4030 energy-dispersive spectroscopy (EDS) detector (Bruker, Billerica, Massachusetts) was used to carry out scanning electron microscopy (SEM) and EDS analysis of the polished sections. SEM was operated in backscattered electron (BSE) mode, 15-kV accelerating voltage, and 12.5-mm working distance. The composition of C-S-H was measured by point EDS analysis on the hydration rims around the hydrated clinker (inner C-S-H) following the method of Rossen and Scrivener (2017). A predefined list of elements (O, Na, Mg, Al, Si, P, S, Cl, K, Ca, Ti, Fe) was used for identification and quantification using $\phi(\rho z)$ correction. A minimum of 200 points were analyzed per sample.

Assessment of Pozzolanic Behavior of Blended Ordinary Portland Cement + SCM Pastes

Paste specimens with 25% SCM replacement levels (water to cementitious material ratio of 0.47) were prepared using electronic mixer and cured for 1 day in a temperature and humidity chamber set at 90% relative humidity and 23°C ± 2°C. After 1 day of curing, the paste specimens were then stored in 1 M NaOH at 80°C for 28 days. Conditions comparable to AMBT were employed to mimic the environment present during accelerated testing. Plain cement paste [ordinary portland cement (OPC)] was also prepared to serve as a reference. Thermogravimetric (TG) data were obtained at 1 and 28 days.

TG curves were obtained using TA Instruments SDT-Q600 (Newcastle, Delaware) simultaneous thermogravimetric analysis/differential scanning calorimetry (TGA/DSC) equipment. The paste specimens were ground using a mortar and pestle and 50-mg sample was taken from the ground material and transferred to a platinum crucible, which was then placed inside the TG instrument. The thermal analysis was performed in a nitrogen gas atmosphere, within a temperature range of 23°C to 1,000°C and at a heating rate of 10°C/min.

Dissolution Tests

Five grams of each SCM type (FA, SL, MK, and SF) was immersed in 50 mL of 1 M NaOH at 80°C for 28 days. Two-milliliter aliquots were pipetted from each mix at 7, 14, 21, and 28 days. All solutions were filtered with 0.2-μm filter to remove any residue, diluted three times with deionized water, and acidified with 120 μL of high-purity nitric acid. Analyses of solutions were carried out through inductively coupled plasma–optical emission spectrometry (ICP-OES) (Shimadzu ICPE-9000, Kyoto, Japan). The concentration of elements in the pore solution was measured at 10×, 100×, and 1,000× dilution of the original sample.

The solid residues in the samples were filtered after 28 days, air-dried, and subjected to SEM-EDS and X-ray diffraction (XRD) to characterize the microstructural and phase changes that occurred in the SCMs. SEM imaging was performed using a Zeiss Supra 55VP SEM (Jena, Germany) fitted with a Bruker SDD EDS Quantax 400 system (Bruker). Phase characterization was carried out using a Bruker D8 Discover XRD in Bragg-Brentano mode using Cu Kα radiation [0.15418 nm (1.5418 Å)]. Diffraction patterns were obtained at a scan rate of 0.04°/s. Phases were identified using DIFFRAC.EVA software version 6 and the ICDD PDF 4+ database. All XRD measurements were performed using a knife edge to minimize background and scattering at low angles.

Results and Discussion

AMBT Expansion Results

AMBT was carried out both at typical Australian SCM replacement levels for effective ASR mitigation and at a fixed SCM dosage of 10% to compare SCM efficacy. Fig. 1 shows AMBT expansion of graywacke mortar without SCM and with different SCMs at typical

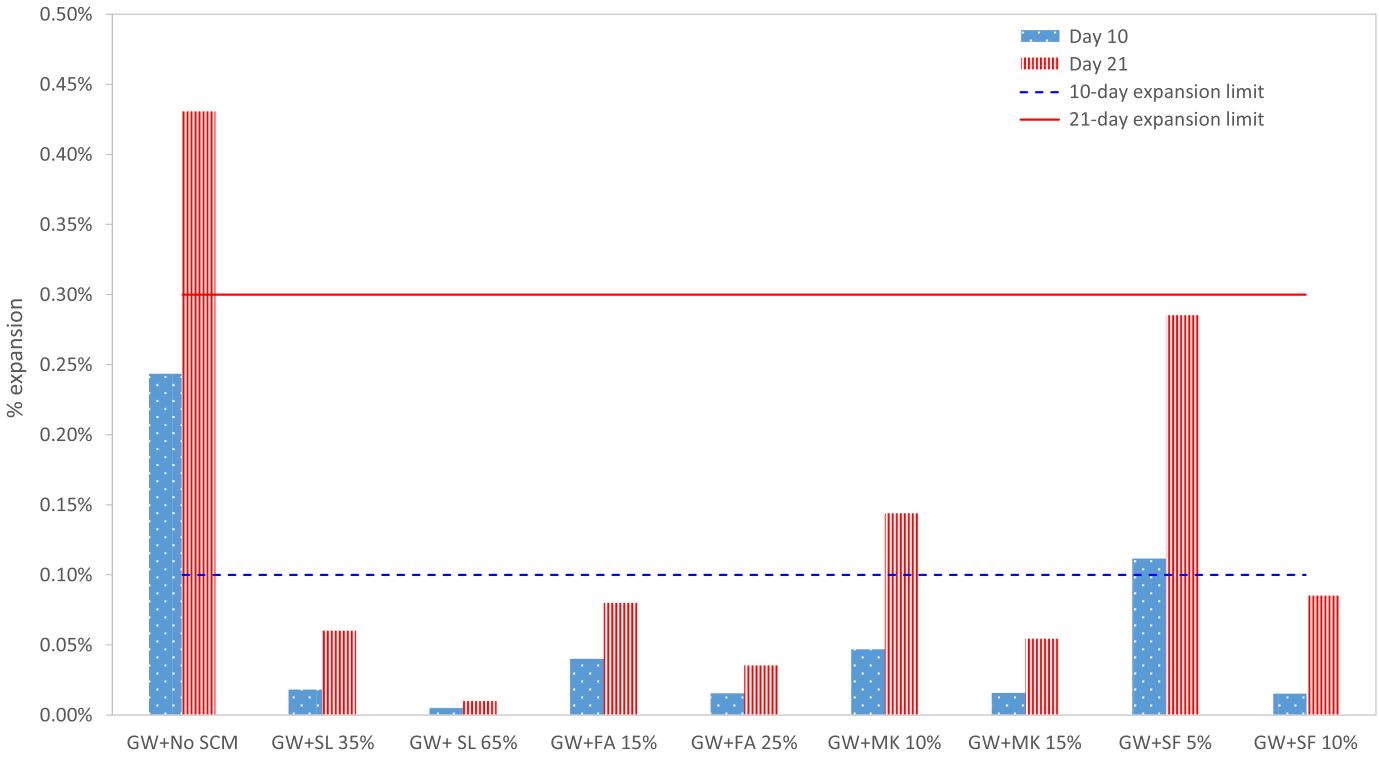

Fig. 1. AMBT expansion of graywacke (GW) aggregate with and without SCMs.

Table 4. Effective reactivity of the mortars based on AS 1141.60.1

Mortar	GW + noSCM	GW + 35% SL	GW + 65% SL	GW + 15% FA	GW + 25% FA	GW + 10% MK	GW + 15% MK	GW + 5% SF	GW + 10% SF
Effective reactivity	R	NR	NR	NR	NR	SR	NR	R	NR

Note: GW = graywacke; R = reactive; SR = slowly reactive; and NR = nonreactive.

dosages used for ASR mitigation (Thomas 2011). The dotted lines at 0.10% and 0.30% correspond to the limits as specified in AS 1141.60.1 (Table 3). The reference mortar with no SCM confirms that graywacke is a reactive aggregate, exceeding both expansion limits at 10 and 21 days. AMBT expansion results of graywacke aggregate with different SCMs at recommended replacement levels show that 10% SF has comparable capacity to reduce ASR expansion to below 0.10% at 10 days and 0.30% at 21 days as 15% FA, 35% SL, and 15% MK. Table 4 summarizes the reactivity of aggregate in each system based on AS 1141.60.1.

Expansion of graywacke mortar specimens in Fig. 2 with 10% replacement of each SCM type showed reduction in ASR expansion in the following order: SF > MK > FA > SL, that is, silica fume generating lowest expansion and slag generating the most. Only the mortar with 10% SL out of all mortars with SCMs exceeded 0.30% expansion at 21 days. Moreover, at 21 days, only SF at 10% replacement level successfully mitigates ASR as per AS 1141.60.1, whereas FA and MK only partially mitigate ASR (slowly reactive systems). The observed effect of SCM on ASR expansion is consistent with field data where silica fume is widely accepted as the best in reducing expansion due to ASR in terms of dosage requirement, closely followed by metakaolin, fly ash, and then blast furnace slag (Thomas 2011). It has been reported that two concretes containing 50% ground-granulated blast-furnace slag (GGBFS) and a ternary blend of 25% slag plus 3.8% silica fume interground with a high-alkali portland cement have neither expanded nor cracked after 20 years (Hooton et al. 2013). Nanty-Moch Dam in the UK and Lower Notch Dam in Ontario, Canada, both built with reactive aggregates and Class F fly ash replacements at 20%–30%, show no signs of ASR at age 50 and 40 years, respectively (Thomas et al. 2012). Fly ash used at replacement levels of 25%–40% was effective in preventing expansion and cracking of large concrete blocks made of three reactive flint sands, highly reactive graywacke aggregates, and a high-alkali (1.15% Na_2O_{eq}) cement for up to 18 years (Thomas et al. 2011). Moreover, a comparative field and laboratory research program initiated at Canada Centre for Mineral and Energy Technology (CANMET) in 1991 showed that marginally and moderately reactive aggregates used in conjunction with high-alkali cement (Na_2O_{eq} > 0.8%) were successfully mitigated by 20% fly ash, 7.5%–12% silica fume, and 35%–65% slag after 15 years of field exposure (expansion level below 0.05%) (Fournier et al. 2016). There are no long-term field data available for metakaolin, but the concrete prism method with two alkali-silica reactive aggregates showed that the amount of high-reactivity metakaolin required to control the expansion to <0.04% at 2 years was found to be between 10% and 15% depending on the aggregate (Ramlochan et al. 2000). All reported literature are consistent with the AMBT results in this study.

Characterization of Mortar Specimens Post-AMBT

In order to better understand the observed expansion, the AMBT specimens with SCMs at recommended replacement levels for ASR

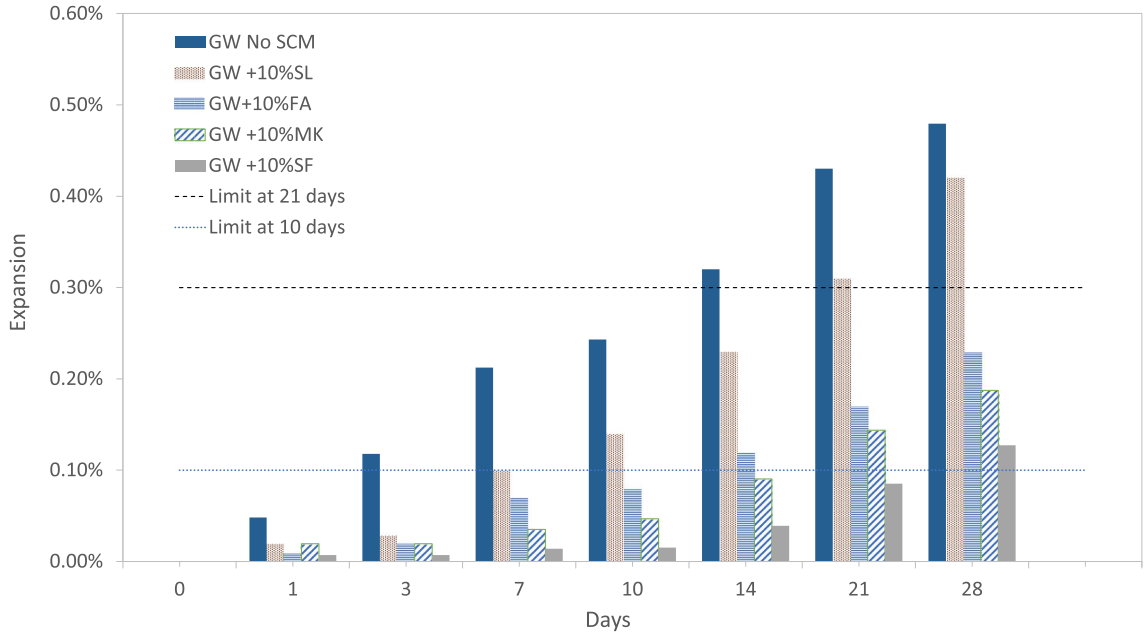

Fig. 2. AMBT expansion of graywacke (GW) aggregate with 10% SCM replacement level (slag, fly ash, metakaolin, and silica fume).

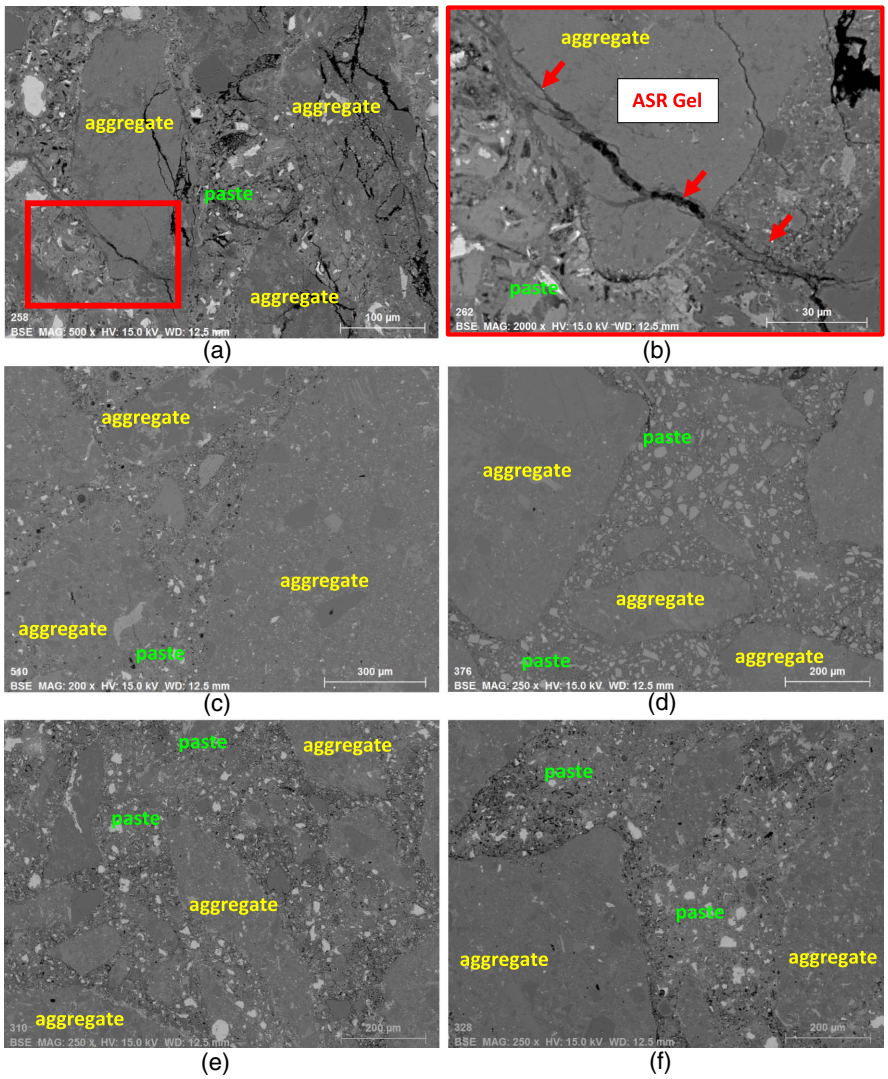

Fig. 3. SEM images of the mortars with (a and b) no SCM; (c) 25% FA; (d) 65% SL; (e) 15% MK; and (f) 10% SF.

J. Mater. Civ. Eng., 2022, 34(3): 04021460

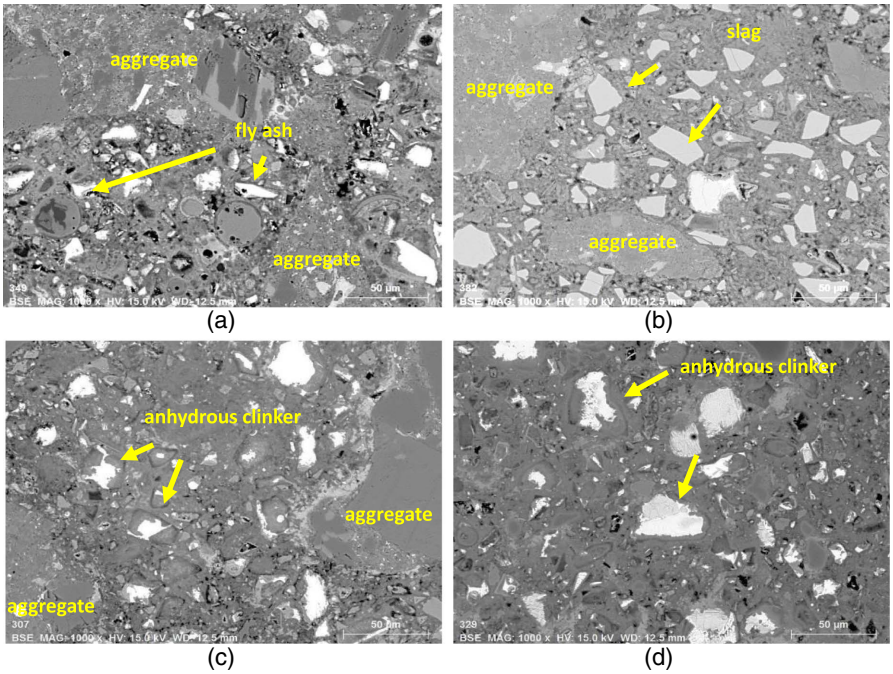

Fig. 4. SEM images of the mortars with (a) 25% FA; (b) 65% SL; (c) 15% MK; and (d) 10% SF showing difference in binder composition.

mitigation (AMBT expansion plotted in Fig. 1) were sectioned and subjected to SEM-EDS analysis. Figs. 3(a and b) show the SEM images of cross-sectioned graywacke mortar specimen without SCM addition post-28 days AMBT. Extensive cracking can be observed in the aggregates, which is consistent with the high degree of expansion during AMBT. Figs. 3(c–e) show low-magnification SEM images of the cross-sectioned graywacke AMBT specimens with SCM additions at typical replacement levels: mortar+ 65% SL, mortar + 25% FA, mortar + 15% MK, and mortar+ 10% SF. All mortar specimens with SCMs show no major cracking in the aggregate or paste.

Fig. 4 shows higher-magnification SEM images of the sectioned mortars. Whereas the angular slag and spherical fly ash particles are still very visible, metakaolin and silica fume are hard to distinguish from the paste. This observation is likely due to the higher reactivity of both MK and SF in the mortar. More anhydrous clinker (bright particles) is still notable in the SF, MK, and FA mortars, likely due to higher cement content than SL mortar.

Fig. 5 shows the C-S-H composition of the mortar specimens. The scatterplots show the effect of 25% FA, 65% SL, 15% MK, and 10% SF on the Ca/Si and Al/Si ratios of C-S-H. All mortars with SCM addition exhibit much higher Si/Ca than pure cement paste (or lower Ca/Si ratio), consistent with that reported in OPC + silica fume and OPC + metakaolin pastes hydrated under ambient curing conditions for 300 days (Chappex and Scrivener 2012a) and OPC + fly ash and OPC + slag concretes immersed in simulated pore solution at 60°C for 6 months (Tapas et al. 2021a). The increase in Si/Ca of the C-S-H with SCM addition is due to silica coming from SCMs (Chappex and Scrivener 2012a). Overlay of the average C-S-H composition of the mortars is shown in Fig. 5(e). The mortar with no SCM addition has an average Si/Ca ratio of 0.57, which is equivalent to a Ca/Si ratio of 1.75. This C-S-H composition agrees with that reported by other studies (Chappex and Scrivener 2012a; Gallucci et al. 2013). Typical values for the Ca/Si ratio of C-S-H in plain cement has been reported to be 1.80–1.90 for both inner and outer C-S-H (Chappex and Scrivener 2012a; Gallucci et al. 2013). The mortars with SCMs have average Si/Ca ratios ranging from 0.62 to 0.68 or Ca/Si ratios of 1.47 to 1.61. Comparable values of Ca/Si ratio obtained for the mortars with SCMs suggests that at the recommended replacement levels, the SCMs are able to contribute almost equivalent amounts of silica to the pore solution and eventually to the C-S-H.

Calcium silicate hydrate with much higher Si/Ca ratio results in higher alkali binding capacity (Thomas 2011). The capacity to bind more alkalis is because of the increase in the amount of acidic silanol (Si-OH) sites in the C-S-H layers that are negatively charged (Duchesne and Berube 1994b; Hong and Glasser 1999). Hence, they attract alkali cations Na^+ and K^+ in the pore solution. The sorption of alkalis increases as the volume of the silanol sites increases. Both the number and acidity of the sites increase as the Ca/Si ratio of C-S-H decreases (Hong and Glasser 2002).

The mortars with 65% SL, 25% FA, and 15% MK showed a significant increase in Al/Si in comparison to the mortar without SCM addition and mortar with 10% SF (Fig. 5). The increase, which is also notably similar, is due to the presence of high amounts of aluminum in slag, metakaolin, and fly ash. This result is consistent with the literature where increasing addition of fly ash, slag, and metakaolin has increased the aluminum in C-S-H (Chappex and Scrivener 2012a, b; Deschner et al. 2013; Taylor et al. 2010). The increase in Al/Si ratio suggests aluminum uptake in C-S-H, which reportedly increases alkali binding capacity. When Al^{3+} substitutes for Si^{4+} in C-S-H, the net charge is negative and therefore the alkali cation (Na^+ or K^+) is bound in order to charge balance, effectively reducing the alkali concentration in the pore solution (Skibsted and Andersen 2013).

Pozzolanic Behavior of SCMs

TG plots of pastes exposed to 1 M NaOH at 80°C storage conditions after 28 days shown as derivative of the mass loss with respect to temperature in Fig. 6 show reduced portlandite (CH) amount in all pastes with SCMs. Mass loss in the range of CH decomposition at about 400°C–500°C corresponds to the dehydroxylation of calcium hydroxide (CH), [$Ca(OH)_2 \rightarrow CaO + H_2O$] (Lothenbach

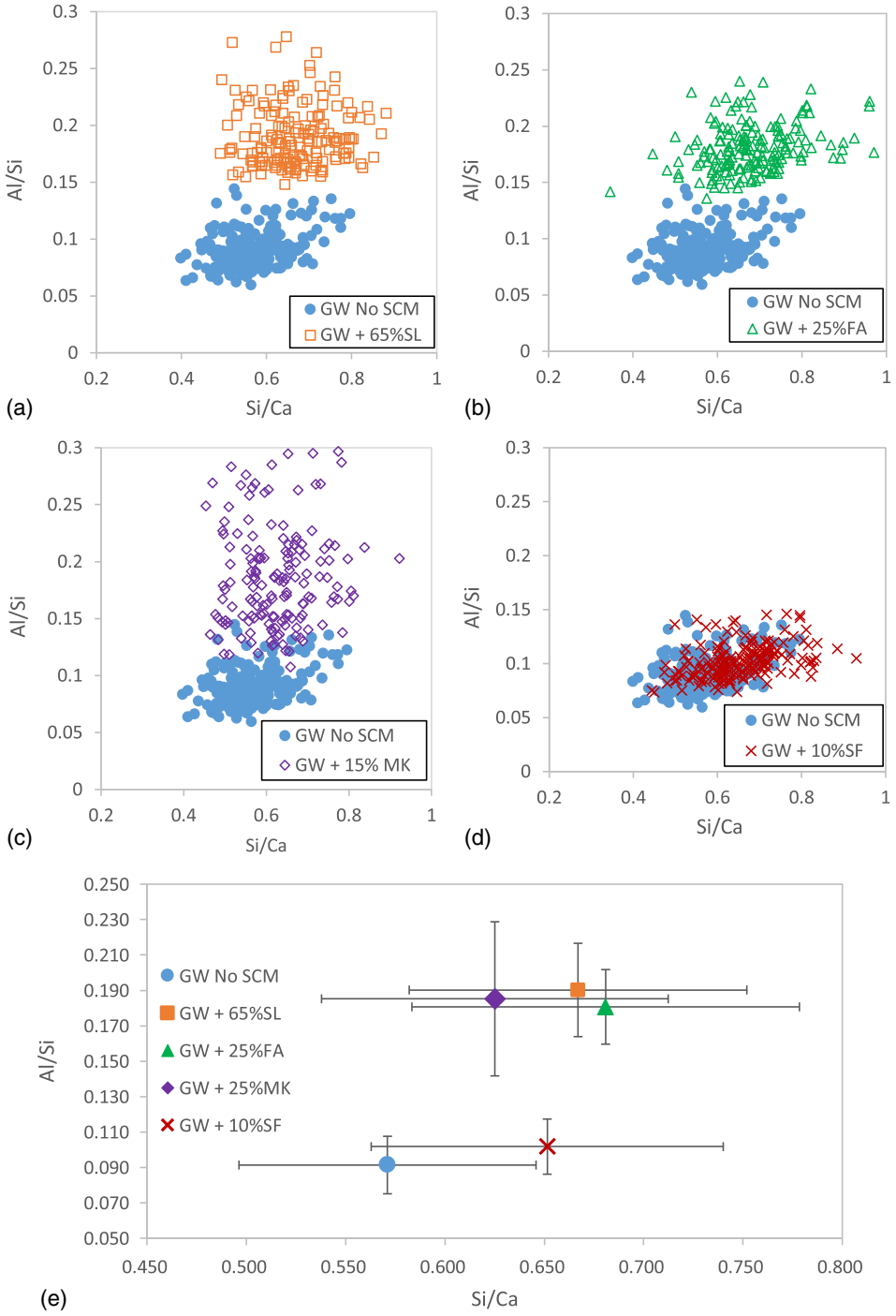

Fig. 5. EDS spot analysis showing the influence of SCM addition at typical replacement levels on C-S-H composition: (a) graywacke + 65% SL; (b) graywacke + 25% FA; (c) graywacke + 15% MK; (d) graywacke + 10% SF; and (e) average Al/Si versus Si/Ca showing one standard deviation distribution for the data plotted in (a–d).

et al. 2016). Therefore, the area under the curve at about 400°C–500°C corresponds to the amount of CH remaining, and thus a larger area means more CH. The reduction in the amount of CH is a combination of cement dilution and of pozzolanic reactions occurring in the binder system. The observed order of portlandite consumption is as follows: OPC + 25% SF > OPC + 25% MK > OPC + 25% FA > OPC + 25% SL, with silica fume being the top consumer of portlandite (most pozzolanic) and slag being the least. The order of portlandite consumption in this study agrees well with other studies that employed accelerated tests to assess pozzolanicity of SCMs (Snellings and Scrivener 2016; Suraneni and Weiss 2017).

From Fig. 6, it can be observed that with the decrease in the amount of portlandite, the area under the curve between 0°C and 200°C increases, which indicates formation of more hydrates (C-S-H) in the system (Lothenbach et al. 2016). Ettringite and carboaluminates are notably absent due to the exposure of the binder systems to higher alkali and temperature conditions (1 M NaOH and 80°C) (Tapas et al. 2021b). Ettringite is known to be unstable at temperature > 70°C as reported in numerous studies

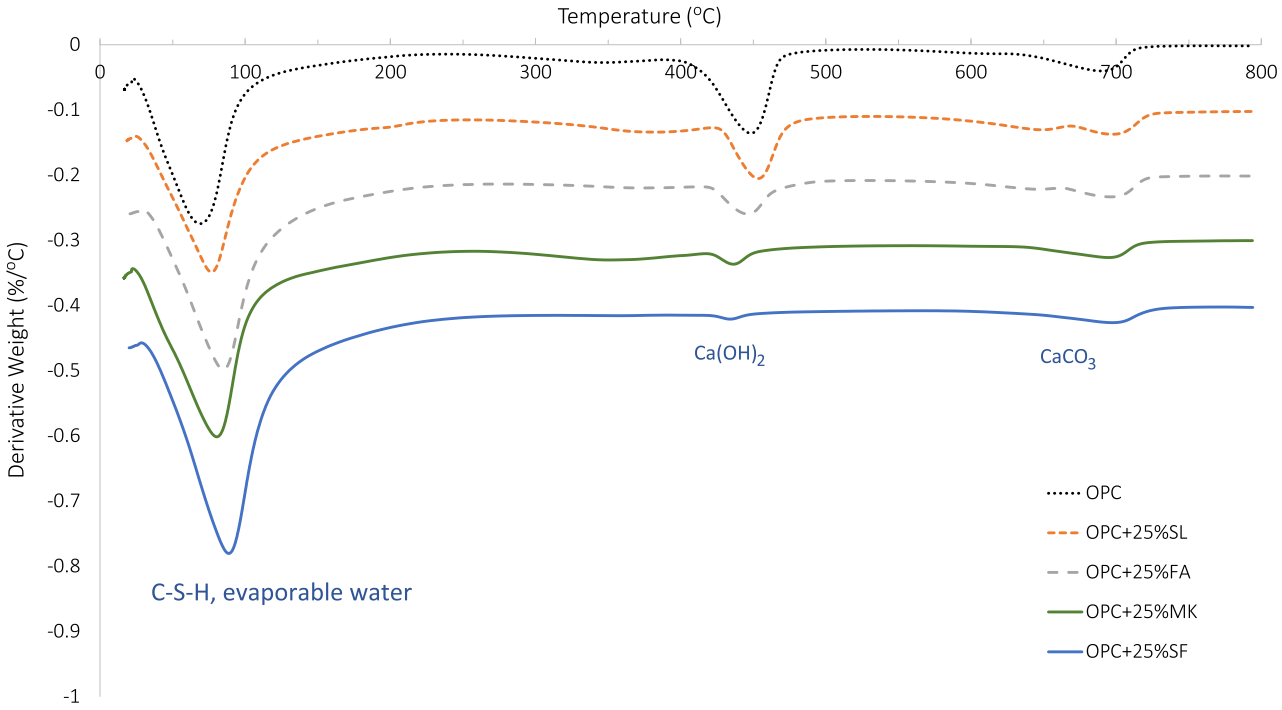

Fig. 6. DTG plot of the hydrated cement-SCM pastes obtained after 28 days immersion in 1 M NaOH at 80°C. DTG = differential thermogravimetry.

(Scrivener and Taylor 1993; Shimada and Young 2004; Taylor et al. 2001). Monocarboaluminates, on the other hand, while stable at temperatures ≥ 70°C, reportedly decompose at temperatures ≥ 90°C (Matschei et al. 2007). The decarbonation of calcite, $CaCO_3$ ($CaCO_3 \rightarrow CaO + CO_2$) occurs between 600°C and 800°C (Lothenbach et al. 2016).

The bar chart in Fig. 7 shows the amount of portlandite in the blended cement pastes immersed in 1 M NaOH at 80°C as a function of age. In agreement with Fig. 6, plain cement (OPC) has the highest amount of portlandite available at 28 days and silica fume the least. Moreover, with the exception of OPC, portlandite was found to decrease with time in all binder systems as a function of time. Slag, which is a latent hydraulic material, is also observed to consume a small amount of portlandite. This observation is consistent with reported values of portlandite consumption by slag, which is generally attributed to slag hydration itself (Escalante et al. 2001; Kolani et al. 2012; Pane and Hansen 2005; Saeki and Monteiro 2005). Slag usually requires an external supply of calcium during hydration to form C-S-H because, relative to cement, slag is calcium deficient. Although the cement used in this study has a $CaO:SiO_2$ ratio of 3:1, slag has almost 1:1. C-S-H generally has a Ca/Si ratio higher than 1.5 (Thomas 2011). Therefore, to form C-S-H, slag in blended cements reacts with calcium from the dissolution of CH formed by the hydration of the cement (Kolani et al. 2012).

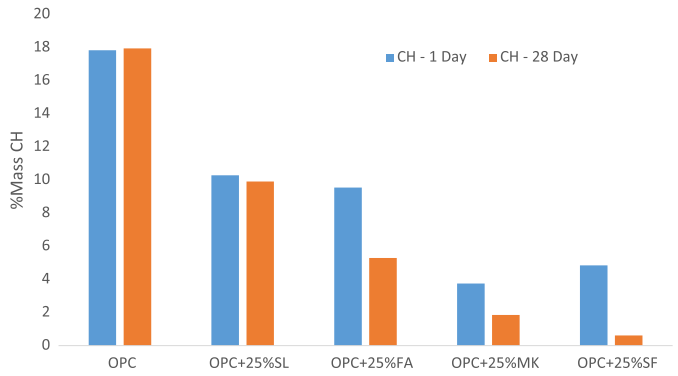

Fig. 7. TG measurements showing percent mass of CH for plain cement and cement with 25% SCM replacement levels at 1 and 28 days.

Pozzolanic reactions are dependent on the presence of reactive silica (SiO_2) in SCMs (Durand et al. 1990; Kim et al. 2015; Thomas 2011). A higher amount of reactive SiO_2 means more reactant available to react with portlandite to produce more negatively charged C-S-H. Silica fume, fly ash, and metakaolin have high contents of soluble silica and thus exhibit a high degree of pozzolanicity.

Higher pozzolanic activity results in a faster production of secondary C-S-H that helps to densify the microstructure and lower the permeability (Thomas 2011). In the absence of SCMs, a higher amount of calcium in the pore solution results in formation of C-S-H with much higher Ca/Si ratio with lower capacity to bind alkalis. Calcium also competes with alkali adsorption in C-S-H. Because Ca^{2+} is more bound than alkalis Na^+ and K^+ in the negatively charged C-S-H, more calcium in the pore solution will decrease the amount of bound alkali in the C-S-H (L'Hôpital et al. 2016).

Dissolution Test Results

In order to assess the degree of reactivity and the rate of delivery of silicate and aluminate ions to the pore solution, slurries of each SCM were prepared in 1 M NaOH and stored at 80°C. Samples for solution concentration analysis were collected at 7, 14, 21, and 28 days and the data are plotted in Fig. 8. The measured concentrations of Si and Al in solution (Fig. 8) represent instantaneous concentrations of these species on extraction of the aliquot of supernatant fluid. The highest concentration of dissolved Si is observed for silica fume, followed by metakaolin, fly ash, and then slag is consistent with that reported in Panagiotopoulou et al. (2007). The amount of Si in solution for fly ash, metakaolin,

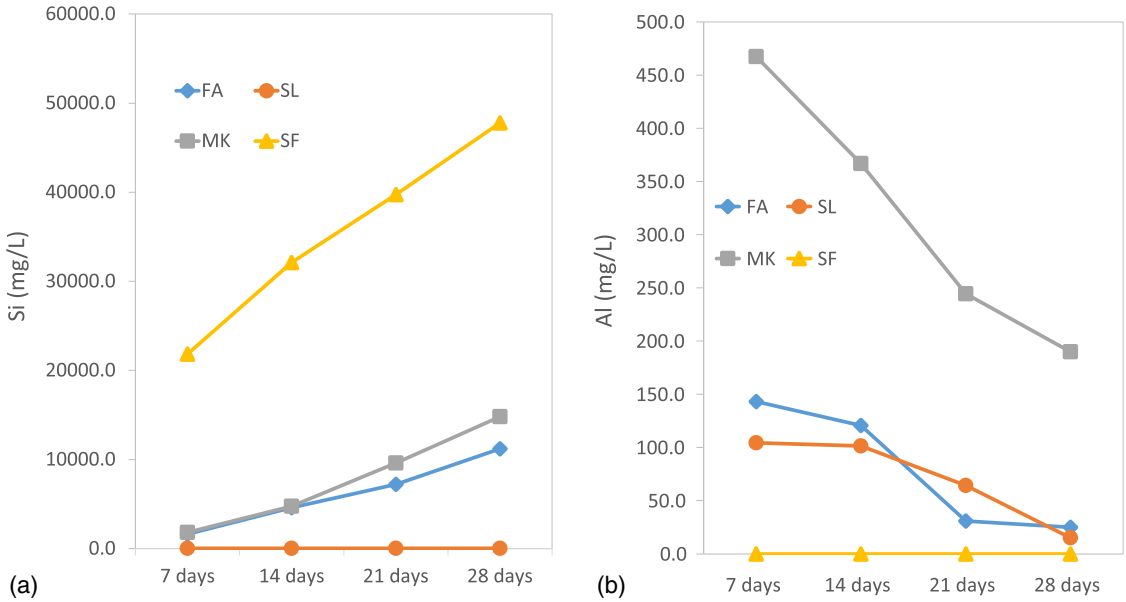

Fig. 8. ICP-OES results showing measured concentrations of (a) silicon (Si); and (b) aluminum (Al) after 7, 14, 21, and 28 days in 1 M NaOH at 80°C.

and slag increases significantly with respect to time. The highest concentration of Si is observed for the silica fume because there is a significant availability of free silica; it is amorphous and therefore reactive. Slag, on the other hand, has very little (almost none) free Si available in solution. The absence of Si in solution for slag implies that all available silica is bound. This means slag has no more excess silica consistent with it being a hydraulic SCM and not pozzolanic.

The amount of available Si in solution measured for all SCMs correlates well with the dosage requirements for effective ASR mitigation (that is, silica fume with the least and slag with the most) and the degree of pozzolanicity as well as the changes observed in the C-S-H composition. Because the formation of C-S-H is affected by the pore solution whose composition is determined by species available in the paste, when the pore solution changes, such as in the case of SCM blends, the composition of C-S-H is expected to change with respect to the dominant species in the pore solution (Rossen et al. 2015). Thus, the increase in Si/Ca and Al/Si ratios observed is due to the release of silicon and aluminum from SCMs into the pore solution.

SCMs with a high proportion of reactive SiO_2 content such as SF, MK, and FA have significant potential in mitigating ASR. Indeed, silica fume, which is almost entirely amorphous silica, generally requires the lowest replacement level among the SCMs at 5%–10%, while slag, which is a calcium-rich SCM, requires the highest dosage to mitigate, normally >50% (Duchesne and Berube 1994a, 2001; Hobbs 1986; Rasheeduzzafar and Hussain 1991). Fly ash and metakaolin release a considerable amount of Si and thus require intermediate amounts (15%–25%) for effective ASR mitigation (Standards Australia 2015).

Aluminum concentration in solution is observed to be in the following order: MK > FA > SL > SF, that is, metakaolin with the highest amount of aluminum in solution followed by fly ash and slag with almost equivalent amounts. This is consistent with another dissolution study of aluminosilicate materials in alkaline media (NaOH and KOH at 2-, 5-, and 10-M concentrations), where metakaolin consistently registers the highest amount of Al in solution followed by fly ash, then slag (Panagiotopoulou et al. 2007). No presence of aluminum in solution was detected for silica fume, consistent with a negligible amount of Al_2O_3 (just 0.1%) in the XRF oxide analysis. Moreover, the aluminum concentration in solution decreases as a function of time, suggesting that aluminum is initially rapidly released, elevating the aluminum concentration, followed by consumption as the aluminosilicate hydrates are formed. The rate of consumption will increase with increasing dissolution of Si. The release of aluminum from FA, MK, and SL under AMBT conditions is also consistent with increased Al/Si ratio in the C-S-H composition of mortars with FA, MK, and SL. The increase in Al/Si ratio suggests aluminum uptake in C-S-H, forming C-A-S-H. When Al^{3+} substitutes for Si^{4+}, this results in a net negative charge and thus an alkali cation (Na^+ or K^+) is bound in the process, leading to further decrease in pore solution alkali concentration.

Fig. 9 shows SEM images and XRD curves of fly ash before and after immersion in 1 M NaOH for 28 days at 80°C. The unreacted fly ash is characterized by spherical particles with a generally smooth texture consistent with the literature [Figs. 9(a and b)] (Fernandez-Jimenez and Palomo 2005; Gebregziabiher et al. 2016). After 28 days in 1 M NaOH solution at 80°C, fleurette-like crystalline structures are observed to coexist with some remaining unreacted spheres [Figs. 9(c and d)], indicating a significant degree of reaction with the development of a new phase.

The XRD pattern of fly ash before alkali immersion in Fig. 9(e) shows the presence of both crystalline and amorphous phases. The major crystalline peaks in the unreacted fly ash were identified as quartz and mullite. The presence of an amorphous phase is indicated by a broad halo in the XRD spectrum centered on 22° 2θ. After 28 days immersion in 1 M NaOH at 80°C, the formation of peaks attributed to N-A-S-H (zeolite, N-Na_2O, A-Al_2O_3, S-SiO_2, H-H_2O) coupled with a further decrease in the intensity of the amorphous halo is observed. The quartz and mullite phases initially present before alkali immersion remain apparently unmodified after 28 days of alkali immersion, indicating that the primary reactant to this point is the amorphous aluminosilicate phase present.

The differences observed in the morphology in the SEM micrographs and the XRD patterns show alkali activation of fly ash at 1 M NaOH at 80°C. At 80°C, zeolite, a crystalline product,

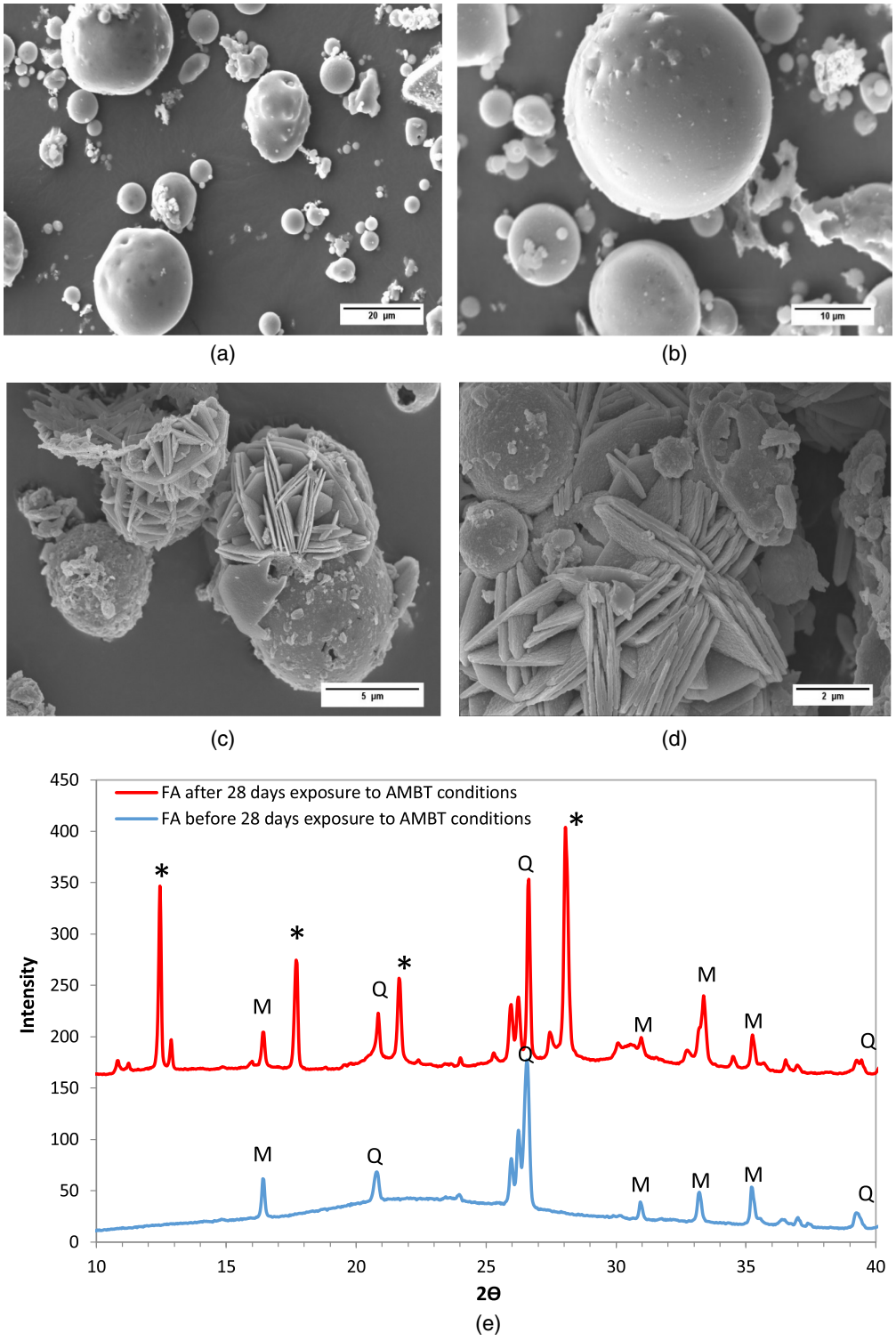

Fig. 9. SEM images of the (a and b) unreacted fly ash; (c and d) fly ash after 28 days immersion in 1 M NaOH at 80°C; and (e) XRD patterns of fly ash before and after 28 days immersion in 1 M NaOH at 80°C. Q = quartz; M = mullite; and * = sodium aluminum silicate hydrate (N A-S-H).

is produced. This is consistent with reported mechanisms of the alkaline activation of fly ash where an X-ray amorphous aluminosilicate gel, a 'zeolite precursor,' is reported to be initially produced, while at elevated temperature crystalline zeolite phases are observed (Fernández-Jiménez et al. 2006a). The two-step process is referred to as the zeolitization process. The significantly elevated temperature provides the necessary reaction environment for the formation of crystalline aluminosilicates and, hence, the zeolitization process is completed, resulting in the observation of the N-A-S-H phase in the XRD (Criado et al. 2007; Fernández-Jiménez et al. 2006a; Fernández-Jiménez and Palomo 2005; Fernández-Jiménez et al. 2006b; Palomo et al. 1999). For both steps of the zeolitization process, the amorphous phases act as the source of the silicate and aluminate ions as the crystalline

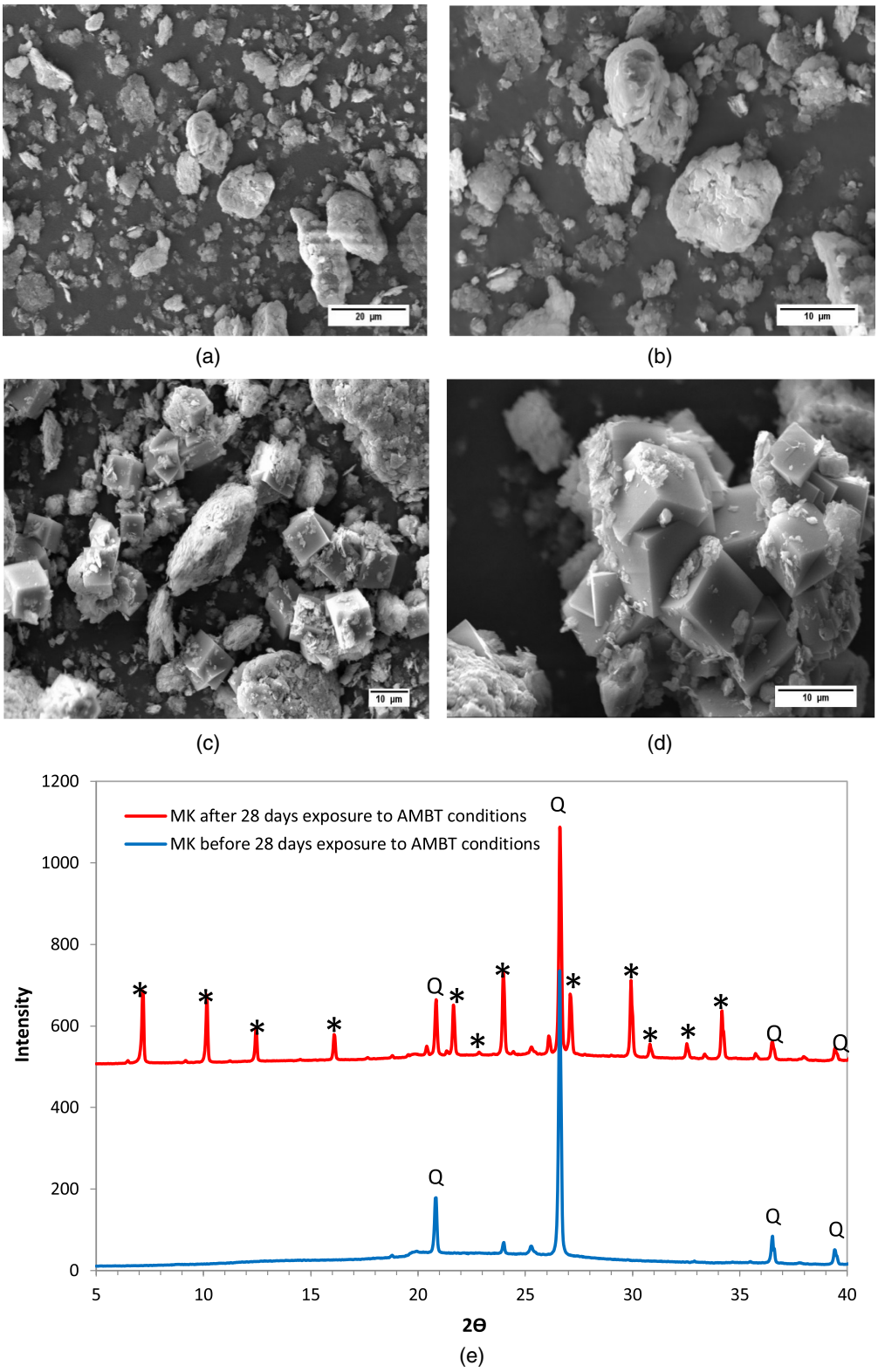

Fig. 10. SEM images of (a and b) unreacted metakaolin; (c and d) metakaolin after 28 days immersion in 1 M NaOH at 80°C; and (e) XRD patterns of metakaolin before and after 28 days immersion in 1 M NaOH at 80°C. Q = quartz; and * = sodium aluminum silicate hydrate (N A-S-H).

phases (mullite and quartz) present in the fly ash typically remain unreactive (Criado et al. 2007; Fernández-Jiménez et al. 2006).

Figs. 10(a–d) show the microstructural changes in metakaolin when immersed in 1 M NaOH at 80°C showing the formation of cubic crystals comparable to those reported by Zhang et al. (2009). XRD results in Fig. 10(e) confirmed the cubic crystals to be N-A-S-H (Type A zeolite, $Na_{96}Al_{96}Si_{96}O_{384} \cdot 216H_2O$), which is consistent with the phases reported for the reaction of metakaolinite with NaOH at elevated temperature (Madani et al. 1990). In a similar stepwise process as that observed with the reaction of fly ash,

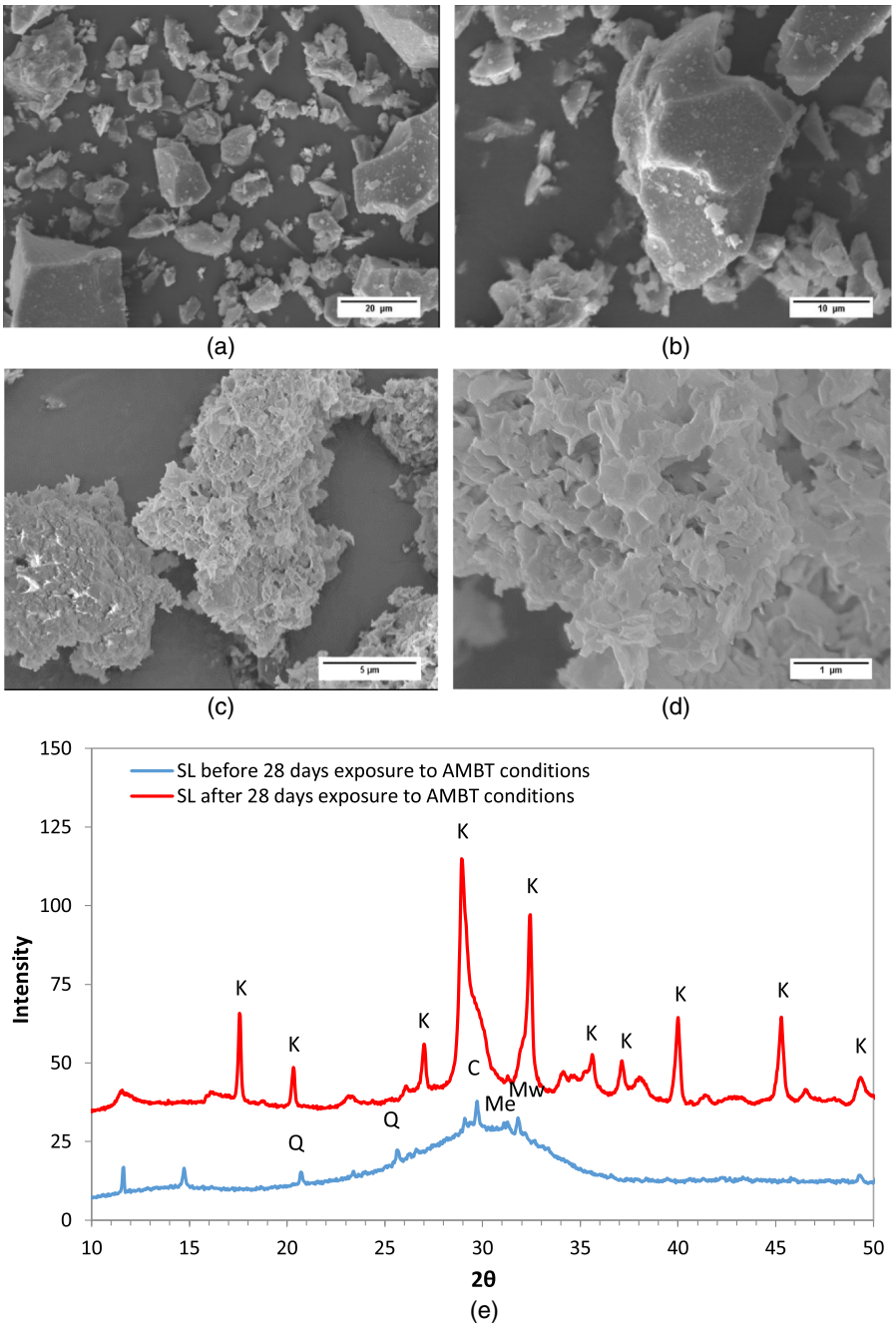

Fig. 11. SEM images of (a and b) unreacted slag; (c and d) slag after 28 days immersion in 1M NaOH at 80°C; and (e) XRD patterns of the slag before and after 28 days immersion in 1 M NaOH at 80°C. Mw = merwinite; Me = melilite; C = calcite; Q = quartz; and K = katoite $(Ca_3Al_2SiO_4)(OH)_8$.

alkaline attack on metakaolin induces the release of silicate and aluminate species in solution that polycondense to form, initially an amorphous aluminosilicate gel that, once formed, converts to Type A zeolite by a structural rearrangement without further change in composition (Zhang et al. 2009).

Figs. 11(a–d) show SEM images of slag before and after 28 days immersion 1 M NaOH at 80°C. Unreacted slag [Figs. 11(a and b)] exhibits angular appearance due to the grinding process and the brittle nature of the glass (Gebregziabiher et al. 2016). The XRD pattern of unreacted slag in Fig. 11(e) shows the presence of a broad halo centered around 30° 2θ, confirming its primarily amorphous/glassy nature (Gebregziabiher et al. 2016). In general, blast-furnace slag may be described as $CaO–SiO_2–Al_2O_3–MgO$ glass (Ye and Radlińska 2016). A change in slag microstructure has been observed [Figs. 11(c and d)], confirming the occurrence of dissolution and formation of a new phase. Development of a platelike microstructure is evident at 80°C. The change in morphology is supported by the formation of a crystalline phase identified as katoite $(Ca_3Al_2SiO_4)(OH)_8$, a form of calcium aluminosilicate hydrate (C-A-S-H) as shown in Fig. 11(e). In a similar fashion to fly ash and metakaolin, slag undergoes dissolution in alkali releasing calcium, aluminum, and silicon ions. However, the products formed from the dissolution of slag are calcium-based (C-A-S-H) rather than sodium-based (N-A-S-H) aluminosilicates, suggesting that the precipitation of calcium aluminosilicates is more favorable. The precipitation of calcium aluminosilicates also allows the sodium

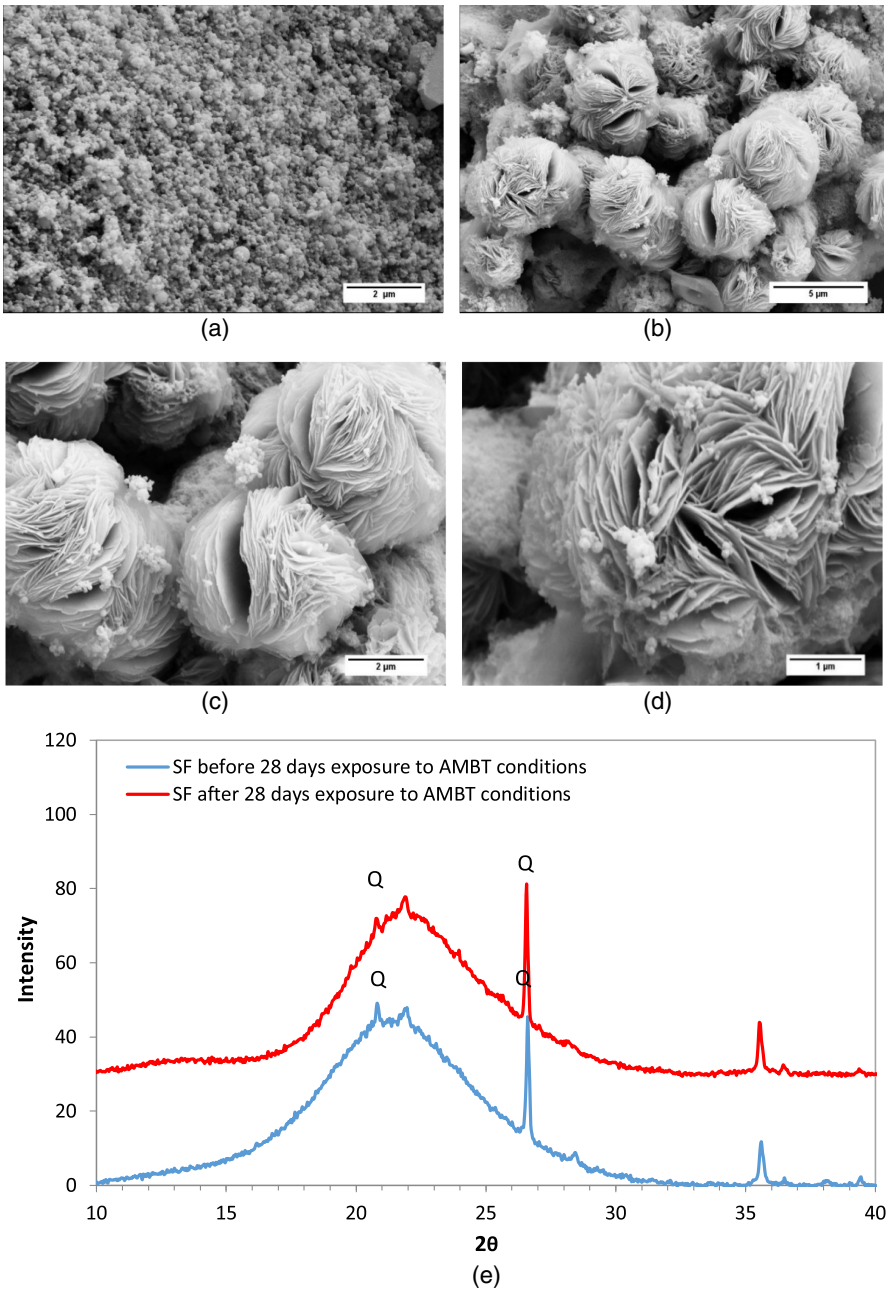

Fig. 12. SEM images of (a) unreacted silica fume; (b–d) silica fume after 28 days immersion in 1 M NaOH at 80°C; and (e) XRD patterns of the silica fume before and after 28 days immersion in 1 M NaOH at 80°C. Q = quartz.

ions to be retained in solution, which, in a cement or concrete context, is effectively a regeneration of the alkalis to the pore solution (Rajabipour et al. 2015). The alkali activation of slag results in the dissolution of silicate and aluminate ions, which aids in the precipitation of C-S-H and C-A-S-H phases (Li et al. 2010). The proportion and type of each phase produced is strongly dependent on the composition of the slag (Tänzer et al. 2015). Under the conditions used in this study, katoite was the major crystalline C-A-S-H phase produced.

The SEM images of unreacted silica fume in Fig. 12(a) show the typical spherical particles in the submicron range (Thomas 2013). After 28 days of immersion in alkali at 80°C, the formation of spherical rosette morphology is observed [Figs. 12(b–d)]. The rosettes have a diameter of approximately 5 μm, which is significantly greater in size than the original spherical particles of the unreacted silica fume, indicating a significant degree of reaction.

The XRD pattern of unreacted silica fume in Fig. 12(e) shows a broad diffraction peak (halo) centered on 22° 2θ, confirming its amorphous nature. Quartz is also observed in the diffraction pattern indicated by the sharp peak at 26.6° 2θ. The features observed in the diffraction pattern of the unreacted silica fume remain largely unchanged after alkali immersion and no crystalline products are observed. The lack of the development of a crystalline phase may be due to the lack of an aluminum source for the precipitation of an aluminosilicate product as is observed for fly ash, metakaolin, and blast-furnace slag.

The aluminum-containing SCMs showed the formation of aluminosilicate hydrates after being exposed to AMBT conditions. FA and MK showed the formation of N-A-S-H (sodium

aluminosilicate hydrate), while slag showed the formation of C-A-S-H (calcium aluminosilicate hydrate). The SCMs can be taken as representative of systems rich in Si (SF), rich in Si and Al (FA and MK), and rich in Si, Al, and Ca (slag). Under an alkali environment, in this case 1 M NaOH, the SCMs dissolve and form reaction products. If aluminum is present, it can bind silicon-forming aluminosilicates (Hünger 2007). Aluminosilicates are negatively charged in a basic environment and therefore attract a cation to charge balance. Thus, Na^+ and Ca^{2+} compete in the process, where Ca^{2+} is preferentially absorbed. Thus, FA and MK form N-A-S-H while slag forms C-A-S-H because it is saturated with calcium. This indicates that in systems with higher calcium contents, fewer alkalis are bound because calcium competes with the alkali (L'Hôpital et al. 2016).

The formation of C-A-S-H in slag and N-A-S-H in fly ash and metakaolin exposed to AMBT conditions is consistent with the expected products that can be formed from the alkali activation of calcium-rich and calcium-poor SCMs, respectively (Wang and Noguchi 2020). In an OPC + SCM binder system, however, calcium is always present due to the presence of cement. Therefore, there will be a constant competition between the formation of C-A-S-H and N-A-S-H and because Ca^{2+} is preferentially bound, C-A-S-H will be the primary product formed. The formation of N-A-S-H will only occur when the available sodium ions in the pore solution far exceed the available calcium such as in the case of AMBT. In this case, the dissolved silica from SCMs will start acting as an alkali sink, effectively reducing pore solution alkali concentration within the mortar bar and preventing ASR expansion. The silica from SCMs are much finer and therefore readily accessible to alkalis and hence are expected to react faster than the silica from the reactive aggregates (Thomas 2011). The efficacy of SCMs to mitigate ASR under AMBT conditions is, however, time limited due to unlimited alkali supply (i.e., eventually the storage solution is expected to dominate the pore solution) (Thomas et al. 2006).

Conclusions

In order to better understand how SCMs mitigate ASR expansion during AMBT, this study investigated the effect of traditional SCMs (FA, SL, MK, and SF) on ASR expansion, composition of the C-S-H phases of mortars post-AMBT, and the consumption of portlandite at an equivalent SCM replacement level. The composition of mortars with different SCMs at recommended dosages for effective ASR mitigation after exposure to AMBT conditions has so far not been compared and reported in the literature. Further, the ability of SCMs to release Si and Al in solution as well as the products formed when SCMs are exposed to AMBT conditions were also investigated to highlight the role of alkali activation and competitive reactions between Ca and Na on ASR mitigation. The following summarizes the important findings from this study:

- Sectioned mortar specimens post-AMBT show extensive cracking in the mortar without SCM and no notable cracks in all mortars with SCMs at typical replacement levels for effective ASR mitigation (25% FA, 65% SL, 15% MK, and 10% SF) consistent with negligible expansion observed. The reduction in expansion observed at the SCM dosages used in this study is consistent with field data reported in literature. Further, the study demonstrates that at an equivalent replacement level of 10%, the order of SCM efficacy is as follows: SF > MK > FA > SL. Portlandite consumption, C-S-H composition, and release of Si and Al from SCMs were investigated to explain the trend in expansion.
- C-S-H composition of mortars post-AMBT shows that all mortars with SCMs have higher Si/Ca ratio than the mortar without SCM. At typical SCM replacement levels for effective ASR mitigation (10% SF, 15% MK, 25% FA, and 65% SL), the change in Si/Ca ratio is comparable, suggesting that at these dosages the SCMs contribute similar amounts of silicon to the pore solution. The Al/Si ratio of C-S-H also increased and is comparable in mortars with 15% MK, 25% FA, and 65% SL. Increases in the Si/Ca and Al/Si ratio of the C-S-H are both associated with increased alkali binding capacity of the C–S-H.
- Cement-SCM blended pastes subjected to TG measurements after 28 days of exposure to AMBT conditions showed that at equivalent replacement dosage of 25%, the order of portlandite consumption is as follows: SF > MK > FA > SL. Silica fume is the most pozzolanic and slag is the least. The order of pozzolanicity is consistent with the efficacy of the SCMs in reducing ASR expansion.
- Solubility studies of SCMs under AMBT conditions show that the ability of SCMs to release Si is as follows: SF > MK > FA > SL, which correlates well with the pozzolanic behavior and the ability of SCMs to reduce ASR expansion. Hence, silicon is the primary factor affecting the efficacy of SCMs in ASR mitigation.
- Microstructure and phase studies of the solid residues confirm formation of aluminosilicate hydrates in all SCMs post exposure to AMBT conditions with the exception of silica fume. Fly ash and metakaolin both formed sodium aluminosilicates (N-A-S-H), whereas slag formed calcium aluminosilicates (C-A-S-H). The dissolution of the SCMs and observed formation of reaction products can also be taken as representative of systems that are (1) rich in silica without aluminum and calcium (silica fume), (2) rich in both silica and aluminum (fly ash and metakaolin), and (3) rich in silica, aluminum, and calcium (slag). Under these conditions, as observed, if aluminum is present, it will bind silicon and take either alkali cations (Na^+ or K^+) or divalent cation Ca^{2+} as a form of charge compensation. If the solution is saturated with calcium, Ca^{2+} is bound instead of alkali. Therefore, the presence of calcium lowers the amount of bound alkali.

A comparable C-S-H Si/Ca ratio of the mortars with varying SCM replacement levels (10% SF, 15% MK, 25% FA, and 65% SL) correlates well with the equivalent efficacy of the SCMs to mitigate ASR at these dosages. The study demonstrates that the changes in C-S-H composition, which is directly related to the release of Si and Al in solution and to the pozzolanic behavior of the SCMs, affects the efficacy of SCMs in mitigating ASR under AMBT conditions. Further, the formation of C-A-S-H in slag and N-A-S-H in fly ash and metakaolin exposed to AMBT conditions highlights the role of alkali activation of SCMs on ASR mitigation. However, the dissolution studies were carried out in 1 M NaOH at 80°C with no external calcium source. In an OPC + SCM binder system, calcium is always present due to the presence of cement. Therefore, there will be a constant competition between the formation of C-A-S-H and N-A-S-H and because Ca^{2+} is preferentially bound, C-A-S-H will be the primary product formed. The formation of N-A-S-H will only occur when the available sodium ions in the pore solution far exceed the available calcium such as in the case of AMBT. In this case, the dissolved silica from SCMs will start acting as an alkali sink, effectively reducing pore solution alkali concentration within the mortar bar and preventing ASR expansion. The efficacy of SCMs to mitigate ASR under AMBT conditions is, however, time limited due to unlimited alkali supply (i.e., eventually the storage solution is expected to dominate the pore solution).

Data Availability Statement

Some or all data, models, or code that support the findings of this study are available from the corresponding author upon reasonable request.

Acknowledgments

This study is a part of University of Technology Sydney research funded through the Australian Research Council Research Hub for Nanoscience-Based Construction Materials Manufacturing (NANOCOMM) with the support of Cement Concrete and Aggregates Australia (CCAA) and the Australian Government Research Training Program Scholarship. This work would also not have been possible without laboratory equipment provided by the Laboratory of Construction Materials at EPFL Switzerland courtesy of Professor Karen Scrivener.

References

ASTM. 1990. *Standard guide for petrographic examination of aggregates for concrete*. ASTM C295. West Conshohocken, PA: ASTM.

ASTM. 2013. *Standard test method for determining the potential alkali-silica reactivity of combinations of cementitious materials and aggregate (accelerated mortar-bar method)*. ASTM C1567. West Conshohocken, PA: ASTM.

ASTM. 2020. *Standard test method for determination of length change of concrete due to alkali-silica reaction*. ASTM C1293. West Conshohocken, PA: ASTM.

Berube, M., J. Duchesne, and D. Chouinard. 1995. "Why the accelerated mortar bar method ASTM C 1260 is reliable for evaluating the effectiveness of supplementary cementing materials in suppressing expansion due to alkali-silica reactivity." *Cem. Concr. Aggregates* 17 (1): 26–34. https://doi.org/10.1520/CCA10333J.

Boddy, A. M., R. D. Hooton, and M. D. A. Thomas. 2003. "The effect of the silica content of silica fume on its ability to control alkali–silica reaction." *Cem. Concr. Res.* 33 (8): 1263–1268. https://doi.org/10.1016/S0008-8846(03)00058-9.

Chappex, T., and K. Scrivener. 2012a. "Alkali fixation of C–S–H in blended cement pastes and its relation to alkali silica reaction." *Cem. Concr. Res.* 42 (8): 1049–1054. https://doi.org/10.1016/j.cemconres.2012.03.010.

Chappex, T., and K. Scrivener. 2012b. "The influence of aluminium on the dissolution of amorphous silica and its relation to alkali silica reaction." *Cem. Concr. Res.* 42 (12): 1645–1649. https://doi.org/10.1016/j.cemconres.2012.09.009.

Criado, M., A. Fernández-Jiménez, A. G. de la Torre, M. A. G. Aranda, and A. Palomo. 2007. "An XRD study of the effect of the SiO_2/Na_2O ratio on the alkali activation of fly ash." *Cem. Concr. Res.* 37 (5): 671–679. https://doi.org/10.1016/j.cemconres.2007.01.013.

Deschner, F., B. Lothenbach, F. Winnefeld, and J. Neubauer. 2013. "Effect of temperature on the hydration of portland cement blended with siliceous fly ash." *Cem. Concr. Res.* 52 (Oct): 169–181. https://doi.org/10.1016/j.cemconres.2013.07.006.

Duchesne, J., and M. A. Berube. 1994a. "The effectiveness of supplementary cementing materials in suppressing expansion due to ASR: Another look at the reaction mechanisms part 1: Concrete expansion and portlandite depletion." *Cem. Concr. Res.* 24 (1): 73–82. https://doi.org/10.1016/0008-8846(94)90084-1.

Duchesne, J., and M. A. Berube. 1994b. "The effectiveness of supplementary cementing materials in suppressing expansion due to ASR: Another look at the reaction mechanisms part 2: Pore solution chemistry." *Cem. Concr. Res.* 24 (2): 221–230. https://doi.org/10.1016/0008-8846(94)90047-7.

Duchesne, J., and M.-A. Berube. 2001. "Long-term effectiveness of supplementary cementing materials against alkali–silica reaction." *Cem. Concr. Res.* 31 (7): 1057–1063. https://doi.org/10.1016/S0008-8846(01)00538-5.

Durand, B., J. Berard, R. Roux, and J. Soles. 1990. "Alkali-silica reaction: The relation between pore solution characteristics and expansion test results." *Cem. Concr. Res.* 20 (3): 419–428. https://doi.org/10.1016/0008-8846(90)90032-S.

Escalante, J. I., L. Y. Gómez, K. K. Johal, G. Mendoza, H. Mancha, and J. Méndez. 2001. "Reactivity of blast-furnace slag in portland cement blends hydrated under different conditions." *Cem. Concr. Res.* 31 (10): 1403–1409. https://doi.org/10.1016/S0008-8846(01)00587-7.

Fernández-Jiménez, A., A. G. de la Torre, A. Palomo, G. López-Olmo, M. M. Alonso, and M. A. G. Aranda. 2006a. "Quantitative determination of phases in the alkaline activation of fly ash. Part II: Degree of reaction." *Fuel* 85 (14): 1960–1969. https://doi.org/10.1016/j.fuel.2006.04.006.

Fernández-Jiménez, A., and A. Palomo. 2005. "Composition and microstructure of alkali activated fly ash binder: Effect of the activator." *Cem. Concr. Res.* 35 (10): 1984–1992. https://doi.org/10.1016/j.cemconres.2005.03.003.

Fernández-Jiménez, A., A. Palomo, I. Sobrados, and J. Sanz. 2006b. "The role played by the reactive alumina content in the alkaline activation of fly ashes." *Microporous Mesoporous Mater.* 91 (1): 111–119. https://doi.org/10.1016/j.micromeso.2005.11.015.

Fournier, B., R. Chevrier, A. Bilodeau, P.-C. Nkinamubanzi, and N. Bouzoubaa. 2016. "Comparative field and laboratory investigations on the use of supplementary cementing materials (SCMs) to control alkali-silica reaction (ASR) in concrete." In *Proc., 15th Int Conf. on Alkali-Aggregate Reaction in Concrete*. Sao Paulo, Brazil: International Conference on Alkali-Aggregate Reaction.

Gallucci, E., X. Zhang, and K. L. Scrivener. 2013. "Effect of temperature on the microstructure of calcium silicate hydrate (C-S-H)." *Cem. Concr. Res.* 53 (Nov): 185–195. https://doi.org/10.1016/j.cemconres.2013.06.008.

Gebregziabiher, B. S., R. J. Thomas, and S. Peethamparan. 2016. "Temperature and activator effect on early-age reaction kinetics of alkali-activated slag binders." *Constr. Build. Mater.* 113 (Jun): 783–793. https://doi.org/10.1016/j.conbuildmat.2016.03.098.

Hobbs, D. W. 1986. "Deleterious expansion of concrete due to alkali-silica reaction: Influence of pfa and slag." *Mag. Concr. Res.* 38 (137): 191–205. https://doi.org/10.1680/macr.1986.38.137.191.

Hong, S.-Y., and F. P. Glasser. 1999. "Alkali binding in cement pastes: Part I. The C-S-H phase." *Cem. Concr. Res.* 29 (12): 1893–1903. https://doi.org/10.1016/S0008-8846(99)00187-8.

Hong, S.-Y., and F. P. Glasser. 2002. "Alkali sorption by C-S-H and C-A-S-H gels: Part II. Role of alumina." *Cem. Concr. Res.* 32 (7): 1101–1111. https://doi.org/10.1016/S0008-8846(02)00753-6.

Hooton, R. D., C. Rogers, C. A. MacDonald, and T. Ramlochan. 2013. "Twenty-year field evaluation of alkali-silica reaction mitigation." *ACI Mater. J.* 110 (5): 539–548.

Hünger, K.-J. 2007. "The contribution of quartz and the role of aluminum for understanding the AAR with greywacke." *Cem. Concr. Res.* 37 (8): 1193–1205. https://doi.org/10.1016/j.cemconres.2007.05.009.

Islam, M. S., M. S. Alam, N. Ghafoori, and R. Sadiq. 2016. "Role of solution concentration, cement alkali and test duration on expansion of accelerated mortar bar test (AMBT)." *Mater. Struct.* 49 (5): 1955–1965. https://doi.org/10.1617/s11527-015-0626-2.

Johnson, S., and K. Chau. 2019. "More U.S. coal-fired power plants are decommissioning as retirements continue." In *Today in energy*. Washington, DC: Energy Information Administration.

Kim, T., J. Olek, and H. Jeong. 2015. "Alkali–silica reaction: Kinetics of chemistry of pore solution and calcium hydroxide content in cementitious system." *Cem. Concr. Res.* 71 (May): 36–45. https://doi.org/10.1016/j.cemconres.2015.01.017.

Kolani, B., L. Buffo-Lacarrière, A. Sellier, G. Escadeillas, L. Boutillon, and L. Linger. 2012. "Hydration of slag-blended cements." *Cem. Concr. Compos.* 34 (9): 1009–1018. https://doi.org/10.1016/j.cemconcomp.2012.05.007.

L'Hôpital, E., B. Lothenbach, K. Scrivener, and D. A. Kulik. 2016. "Alkali uptake in calcium alumina silicate hydrate (C-A-S-H)." *Cem. Concr. Res.* 85 (Jul): 122–136. https://doi.org/10.1016/j.cemconres.2016.03.009.

Li, C., H. Sun, and L. Li. 2010. "A review: The comparison between alkali-activated slag (Si+Ca) and metakaolin (Si+Al) cements." *Cem. Concr. Res.* 40 (9): 1341–1349. https://doi.org/10.1016/j.cemconres.2010.03.020.

Lothenbach, B., P. Durdziński, and K. D. Weerdt. 2016. "A practical guide to microstructural analysis of cementitious materials." In *Thermogravimetric analysis*, edited by K. Scrivener, R. Snellings, and B. Lothenbach. Oxford, UK: Taylor & Francis.

Lothenbach, B., K. Scrivener, and R. D. Hooton. 2011. "Supplementary cementitious materials." *Cem. Concr. Res.* 41 (12): 1244–1256. https://doi.org/10.1016/j.cemconres.2010.12.001.

Madani, A., A. Aznar, J. Sanz, and J. M. Serratosa. 1990. "29Si and 27Al NMR study of zeolite formation from alkali-leached kaolinites. Influence of thermal preactivation." *J. Phys. Chem.* 94 (2): 760–765. https://doi.org/10.1021/j100365a046.

Matschei, T., B. Lothenbach, and F. P. Glasser. 2007. "Thermodynamic properties of portland cement hydrates in the system $CaO–Al_2O_3–SiO_3–CaSO_4–CaCO_3–H_2O$." *Cem. Concr. Res.* 37 (10): 1379–1410. https://doi.org/10.1016/j.cemconres.2007.06.002.

Nalbandian-Sugden, H. 2015. *New regulatory trends: Effects on coal-fired power plants and coal demand*. London: IEA Clean Coal Centre.

Palomo, A., M. W. Grutzeck, and M. T. Blanco. 1999. "Alkali-activated fly ashes: A cement for the future." *Cem. Concr. Res.* 29 (8): 1323–1329. https://doi.org/10.1016/S0008-8846(98)00243-9.

Panagiotopoulou, C., E. Kontori, T. Perraki, and G. Kakali. 2007. "Dissolution of aluminosilicate minerals and by-products in alkaline media." *J. Mater. Sci.* 42 (9): 2967–2973. https://doi.org/10.1007/s10853-006-0531-8.

Pane, I., and W. Hansen. 2005. "Investigation of blended cement hydration by isothermal calorimetry and thermal analysis." *Cem. Concr. Res.* 35 (6): 1155–1164. https://doi.org/10.1016/j.cemconres.2004.10.027.

Rajabipour, F., E. Giannini, C. Dunant, J. H. Ideker, and M. D. A. Thomas. 2015. "Alkali–silica reaction: Current understanding of the reaction mechanisms and the knowledge gaps." *Cem. Concr. Res.* 76 (Oct): 130–146. https://doi.org/10.1016/j.cemconres.2015.05.024.

Ramlochan, T., M. Thomas, and K. A. Gruber. 2000. "The effect of metakaolin on alkali-silica reaction in concrete." *Cem. Concr. Res.* 30 (3): 339–344. https://doi.org/10.1016/S0008-8846(99)00261-6.

Rasheeduzzafar, S., and S. E. Hussain. 1991. "Effect of microsilica and blast furnace slag on pore solution composition and alkali-silica reaction." *Cem. Concr. Compos.* 13 (3): 219–225. https://doi.org/10.1016/0958-9465(91)90023-B.

Rossen, J. E., B. Lothenbach, and K. L. Scrivener. 2015. "Composition of C–S–H in pastes with increasing levels of silica fume addition." *Cem. Concr. Res.* 75 (Sep): 14–22. https://doi.org/10.1016/j.cemconres.2015.04.016.

Rossen, J. E., and K. L. Scrivener. 2017. "Optimization of SEM-EDS to determine the C–A–S–H composition in matured cement paste samples." *Mater. Charact.* 123 (Jan): 294–306. https://doi.org/10.1016/j.matchar.2016.11.041.

Saeki, T., and P. J. M. Monteiro. 2005. "A model to predict the amount of calcium hydroxide in concrete containing mineral admixtures." *Cem. Concr. Res.* 35 (10): 1914–1921. https://doi.org/10.1016/j.cemconres.2004.11.018.

Scrivener, K. L., V. M. John, and E. M. Gartner. 2016. *Eco-efficient cements: Potential, economically viable solutions for a low* CO_2 *cement-based materials industry.* Washington, DC: United Nations Environment Program.

Scrivener, K. L., and H. F. W. Taylor. 1993. "Delayed ettringite formation: A microstructural and microanalytical study." *Adv. Cem. Res.* 5 (20): 139–146. https://doi.org/10.1680/adcr.1993.5.20.139.

Shafaatian, S. M. H., A. Akhavan, H. Maraghechi, and F. Rajabipour. 2013. "How does fly ash mitigate alkali–silica reaction (ASR) in accelerated mortar bar test (ASTM C1567)?" *Cem. Concr. Compos.* 37 (Mar): 143–153. https://doi.org/10.1016/j.cemconcomp.2012.11.004.

Shimada, Y., and J. F. Young. 2004. "Thermal stability of ettringite in alkaline solutions at 80°C." *Cem. Concr. Res.* 34 (12): 2261–2268. https://doi.org/10.1016/j.cemconres.2004.04.008.

Sirivivatnanon, V., J. Mohammadi, and W. South. 2016. "Reliability of new Australian test methods in predicting alkali silica reaction of field concrete." *Constr. Build. Mater.* 126 (Nov): 868–874. https://doi.org/10.1016/j.conbuildmat.2016.09.055.

Skibsted, J., and M. D. Andersen. 2013. "The effect of alkali ions on the incorporation of aluminum in the calcium silicate hydrate (C–S–H) phase resulting from portland cement hydration studied by ^{29}Si MAS NMR." *J. Am. Ceram. Soc.* 96 (2): 651–656. https://doi.org/10.1111/jace.12024.

Snellings, R., and K. L. Scrivener. 2016. "Rapid screening tests for supplementary cementitious materials: Past and future." *Mater. Struct.* 49 (8): 3265–3279. https://doi.org/10.1617/s11527-015-0718-z.

Standards Australia. 2014a. *Aggregates and rock for engineering purposes*. AS 2758.1. Sydney, Australia: Standards Australia.

Standards Australia. 2014b. *Methods for sampling and testing aggregates method 60.1: Potential alkali-silica reactivity-accelerated mortar bar method*. AS 1141.60.1. Sydney, Australia: Standards Australia.

Standards Australia. 2014c. *Methods for sampling and testing aggregates method 60.2: Potential alkali-silica reactivity-concrete prism method*. AS 1141.60.2. Sydney, Australia: Standards Australia.

Standards Australia. 2015. *Alkali aggregate reaction—Guidelines on minimising the risk of damage to concrete structures in Australia*. SA HB 79:2015. Sydney, Australia: Standards Australia.

Suraneni, P., and J. Weiss. 2017. "Examining the pozzolanicity of supplementary cementitious materials using isothermal calorimetry and thermogravimetric analysis." *Cem. Concr. Compos.* 83 (Oct): 273–278. https://doi.org/10.1016/j.cemconcomp.2017.07.009.

Tänzer, R., A. Buchwald, and D. Stephan. 2015. "Effect of slag chemistry on the hydration of alkali-activated blast-furnace slag." *Mater. Struct.* 48 (3): 629–641. https://doi.org/10.1617/s11527-014-0461-x.

Tapas, M. J., L. Sofia, K. Vessalas, P. Thomas, V. Sirivivatnanon, and K. Scrivener. 2021a. "Efficacy of SCMs to mitigate ASR in systems with higher alkali contents assessed by pore solution method." *Cem. Concr. Res.* 142 (Apr): 106353. https://doi.org/10.1016/j.cemconres.2021.106353.

Tapas, M. J., K. Vessalas, P. Thomas, and V. Sirivivatnanon. 2021b. "Influence of limestone mineral addition in cements on the efficacy of SCMs in mitigating alkali-silica reaction assessed by accelerated mortar bar test." *J. Mater. Civ. Eng.* 33 (6): 04021106. https://doi.org/10.1061/(ASCE)MT.1943-5533.0003728.

Taylor, H., C. Famy, and K. Scrivener. 2001. "Delayed ettringite formation." *Cem. Concr. Res.* 31 (5): 683–693. https://doi.org/10.1016/S0008-8846(01)00466-5.

Taylor, R., I. G. Richardson, and R. M. D. Brydson. 2010. "Composition and microstructure of 20-year-old ordinary portland cement–ground granulated blast-furnace slag blends containing 0 to 100% slag." *Cem. Concr. Res.* 40 (7): 971–983. https://doi.org/10.1016/j.cemconres.2010.02.012.

Thomas, M. 2011. "The effect of supplementary cementing materials on alkali-silica reaction: A review." *Cem. Concr. Res.* 41 (12): 1224–1231. https://doi.org/10.1016/j.cemconres.2010.11.003.

Thomas, M., B. Fournier, K. Folliard, J. Ideker, and M. Shehata. 2006. "Test methods for evaluating preventive measures for controlling expansion due to alkali–silica reaction in concrete." *Cem. Concr. Res.* 36 (10): 1842–1856. https://doi.org/10.1016/j.cemconres.2006.01.014.

Thomas, M., R. D. Hooton, C. Rogers, and B. Fournier. 2012. "50 years old and still going strong: Fly ash puts paid to ASR." *Concr. Int.* 34 (1): 35–40.

Thomas, M. D. A. 2013. *Supplementary cementing materials in concrete*. Boca Raton, FL: Taylor & Francis.

Thomas, M. D. A., A. Dunster, P. Nixon, and B. Blackwell. 2011. "Effect of fly ash on the expansion of concrete due to alkali-silica reaction—Exposure site studies." *Cem. Concr. Compos.* 33 (3): 359–367. https://doi.org/10.1016/j.cemconcomp.2010.11.006.

Thomas, M. D. A., B. Fournier, K. J. Folliard, M. H. Shehata, J. H. Ideker, and A. C. Rogers. 2007. "Performance limits for evaluating supplementary cementing materials using accelerated mortar bar test." *ACI Mater. J.* 2005 (3): 115–122. https://doi.org/10.14359/18573.

Wang, W., and T. Noguchi. 2020. "Alkali-silica reaction (ASR) in the alkali-activated cement (AAC) system: A state-of-the-art review." *Constr. Build. Mater.* 252 (Aug): 119105. https://doi.org/10.1016/j.conbuildmat.2020.119105.

Ye, H., and A. Radlińska. 2016. "Quantitative analysis of phase assemblage and chemical shrinkage of alkali-activated slag." *J. Adv. Concr. Technol.* 14 (5): 245–260. https://doi.org/10.3151/jact.14.245.

Zhang, B., K. J. D. MacKenzie, and I. W. M. Brown. 2009. "Crystalline phase formation in metakaolinite geopolymers activated with NaOH and sodium silicate." *J. Mater. Sci.* 44 (17): 4668–4676. https://doi.org/10.1007/s10853-009-3715-1.